Bull. Soc. R. Sci. Liège, 2024, **93**(2), 453–460 *Peer-reviewed conference paper*
doi:10.25518/0037-9565.11747

Abundances of Extreme r-Process Elements in a Sample of CEMP-rs Stars

Muhammed RIYAS[1], Drisya KARINKUZHI[1,2,*] and Sophie VAN ECK[2,*]

[1] Department of Physics, University of Calicut, Kerala–673635, India.
[2] Institut d'Astronomie et d'Astrophysique, Université Libre de Bruxelles, ULB, Campus Plaine C. P. 226, Boulevard du Triomphe, 1050 Bruxelles, Belgium.
[*] Corresponding authors: drdrisyak@uoc.ac.in, svaneck@astro.ulb.ac.be

Paper presented at the 3rd BINA Workshop on "Scientific Potential of the Indo-Belgian Cooperation", held at the Graphic Era Hill University, Bhimtal (India), 22nd–24th March 2023.

Abstract

We analyze high-resolution spectra of five carbon-enhanced metal-poor (CEMP) stars acquired using Ultraviolet and Visual Echelle Spectrograph (UVES). Assuming local thermodynamic equilibrium (LTE), we derive the abundances of extreme r-process elements such as Tb, Ho, Tm, and Yb using TURBOSPECTRUM radiative transfer code with MARCS model atmospheres. Four of the program stars have their atmospheric parameters adopted from our previous studies, while for CS 22947-187, we determine the atmospheric parameters ($T_{\rm eff} = 5200$ K, $\log g = 1.5$, $\xi = 1.70\,{\rm km\,s^{-1}}$, and [Fe/H] $= -2.55$) using the BACCHUS code in semi-automated mode. These stars are already classified as CEMP-rs stars (i.e., carbon-enhanced metal-poor stars with enrichment of elements from both slow and rapid neutron-capture processes), using our new classification criteria for CEMP stars. The derived r-process abundances for our program stars are similar to those for rI and rII stars of similar metallicity.

Keywords: Nuclear reactions, nucleosynthesis, abundances – Stars: AGB and post-AGB – binaries: spectroscopic

1. Introduction

Understanding the production of chemical elements by stellar nucleosynthesis and their re-distribution in the Galaxy, the so-called galactic chemical evolution (GCE), is an important topic in modern astronomy. Our understanding of the galactic abundance of the elements, however, remains incomplete because of major uncertainties, such as the contribution from different nucleosynthetic processes. Furthermore, the origin of the peculiar abundance patterns shown by specific stellar subgroups are still not well understood in many aspects. One example concerns carbon-enhanced metal-poor (CEMP) stars showing enhancement of elements both from the slow-neutron capture process (s-process) and the rapid neutron capture process (r-process). They are also known as CEMP-rs stars. According to recent studies (Karinkuzhi

et al., 2021a, 2020; Hampel et al., 2019, 2016), the intermediate neutron-capture process (i-process) that occurs in low-metallicity, low-mass thermally pulsing Asymptotic Giant Branch stars is most likely responsible for the peculiar abundance in CEMP-rs stars. Studies such as these demonstrated a satisfactory match between measured abundances in CEMP-rs stars and model predictions. However, detailed abundances of large samples of CEMP-rs stars at different metallicities are required to gain a deep understanding of the i-process.

The detailed abundances of eleven CEMP-rs stars derived using the high-resolution HERMES spectra were presented in our previous study (Karinkuzhi et al., 2021a). The measured abundances in these stars were satisfactorily explained by the i-process occurring in thermally pulsing (TP)–AGB stars after proton ingestion during their first convective thermal pulse (Choplin et al., 2021). However, the abundances of extreme r-process elements such as Tb, Ho, Tm, and Yb were not considered in this study as they were not measurable since their sensitive lines are beyond the HERMES wavelength limits. Nonetheless, it is important to identify the role that the i-process plays in the production of extreme r-process elements in general, as well as its contribution to the chemical enrichment of our galaxy. Studies such as these can provide important constraints for galactic chemical evolution models.

2. Data and Analysis

The UVES spectra for our objects cover a wavelength of 3280 to 6835 Å. The atmospheric parameters, $T_{\rm eff}$, $\log g$, ξ, and [Fe/H] are derived using the BACCHUS code in semi-automated mode as described in Karinkuzhi et al. (2018, 2021a,b). Abundances were derived by comparing the observed spectrum with the synthetic one generated with the TURBOSPECTRUM radiative transfer code (Alvarez and Plez, 1998) using MARCS model atmospheres. The solar abundances were adopted from Asplund et al. (2009). The line lists from Heiter et al. (2015) and Heiter (2020) were used for deriving the individual elemental abundances. The Local Thermodynamic Equilibrium (LTE) conditions were assumed for deriving the abundances, but non-LTE (NLTE) corrections were applied when available. For all the elements except Ho, Tb, Tm, and Yb, the derivation of the elemental abundances has already been discussed in Karinkuzhi et al. (2021a). Here we describe only the extreme r-process elements.

2.1. r-process elements: Tb, Ho, Tm, Yb

We measured the abundance of Tb, Ho, Tm, and Yb in all the program stars. They are presented in Table 1. There are several lines available for the elements Tm and Ho in the wavelength range of 3700 to 3900 Å. They are listed in Table 2. This region is a bit noisy but we could measure their abundance using two or three lines for Ho and Tm in all the stars except for HD 196944, where Tm abundance is derived using a single Tm II line. The Yb and Tb abundances were derived using the lines at 3694.19 and 3845.63 Å respectively. We present the spectral synthesis of the Tm II line at 3795.76 Å and theYb II line at 3694.19 Å in Fig. 1 for two program stars. The uncertainties in abundance were derived as discussed in Karinkuzhi et al. (2018). The atmospheric parameters $T_{\rm eff}$, $\log g$, microturbulence ξ, and [Fe/H] are varied by

Table 1: Elemental abundances. The values for $\log_{\odot} \varepsilon$ are taken from Asplund et al. (2009) and : indicates the upper limit.

	Z	$\log_{\odot} \varepsilon$	$\log \varepsilon$	σ_{l}**(N)**	**[X/Fe]** $\pm \sigma_{\mathrm{t}}$
CS 22947–187					
Tb	65	0.30	−0.90	0.10(1)	1.35 ± 0.45
Ho	67	0.48	−1.57	0.03(2)	0.50 ± 0.09
Tm	69	0.10	−1.25	0.04(3)	1.20 ± 0.09
Yb	70	0.84	−0.65	0.10(1)	1.06 ± 0.11
CS 22891–171					
Tb	65	0.30	−0.70	0.06(3)	1.50 ± 0.44
Ho	67	0.48	−0.98	0.04(4)	1.04 ± 0.08
Tm	69	0.10	−0.75	0.04(3)	1.65 ± 0.09
Yb	70	0.84	−0.50	0.10(1)	1.16 ± 0.11
HD 187861					
Tb	65	0.30	−1.00	0.10(2)	1.30 ± 0.45
Ho	67	0.48	−1.03	0.07(4)	1.09 ± 0.09
Tm	69	0.10	−0.95	0.05(2)	1.55 ± 0.10
Yb	70	0.84	−0.60	0.10(1)	1.16 ± 0.11
HD 224959					
Tb	65	0.30	−0.57	0.08(4)	1.49 ± 0.44
Ho	67	0.48	−0.30	0.05(2)	1.58 ± 0.09
Tm	69	0.10	−0.20	0.04(3)	2.06 ± 0.09
Yb	70	0.84	0.20	0.10(1)	1.72 ± 0.11
HD 196944					
Tb	65	0.30	−0.58:	0.05(2)	1.62 ± 0.45
Ho	67	0.48	−2.00	0.10(2)	0.02 ± 0.11
Tm	69	0.10	−1.60	0.10(1)	0.80 ± 0.13
Yb	70	0.84	−0.90	0.10(1)	0.76 ± 0.11

Table 2: Lines used in the abundance analysis.

λ (Å)	$\chi_{\rm low}$ (eV)	$\log gf$
Tb II		
3658.888	0.126	−4.083
3702.869	0.126	−1.671
3775.268	0.790	−0.570
3845.633	0.790	0.252
3848.744	0.000	−0.317
3899.188	0.373	0.330
4002.566	0.641	0.100
4005.467	0.126	−0.020
Ho II		
3453.123	0.079	−0.930
3456.020	0.000	−2.828
3484.816	0.079	−0.636
3796.754	0.000	−1.722
3810.738	0.000	0.142
4045.470	0.000	−0.918
4152.586	0.079	−2.733
Tm II		
3700.255	0.029	−0.380
3701.362	0.000	−0.540
3734.123	0.029	−0.710
3795.759	0.029	−0.230
Yb II		
3694.192	0.000	−0.300

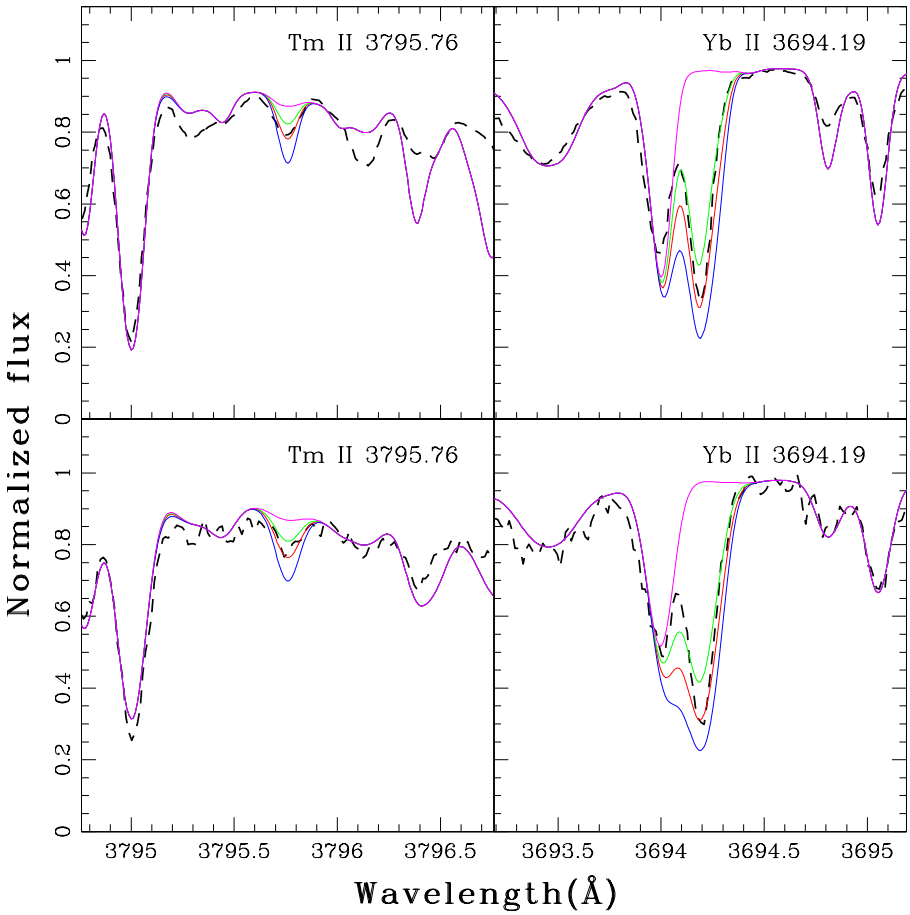

Figure 1: Spectral fitting of the Tm II and Yb II lines is shown for two CEMP-rs stars, HD 196944 and CS22947−187 in the upper and lower panels respectively. Red lines correspond to spectral syntheses with the adopted Tm II, Yb II abundances of −1.6 dex, −0.9 dex for HD196944, and −1.25 dex, −0.7 dex for CS22947–187 respectively. Blue and green lines correspond to syntheses with abundances deviating by ±0.3 dex from the adopted abundance. The black dashed line represents the observed spectrum. The magenta line corresponds to the synthesis with a null abundance for the corresponding element.

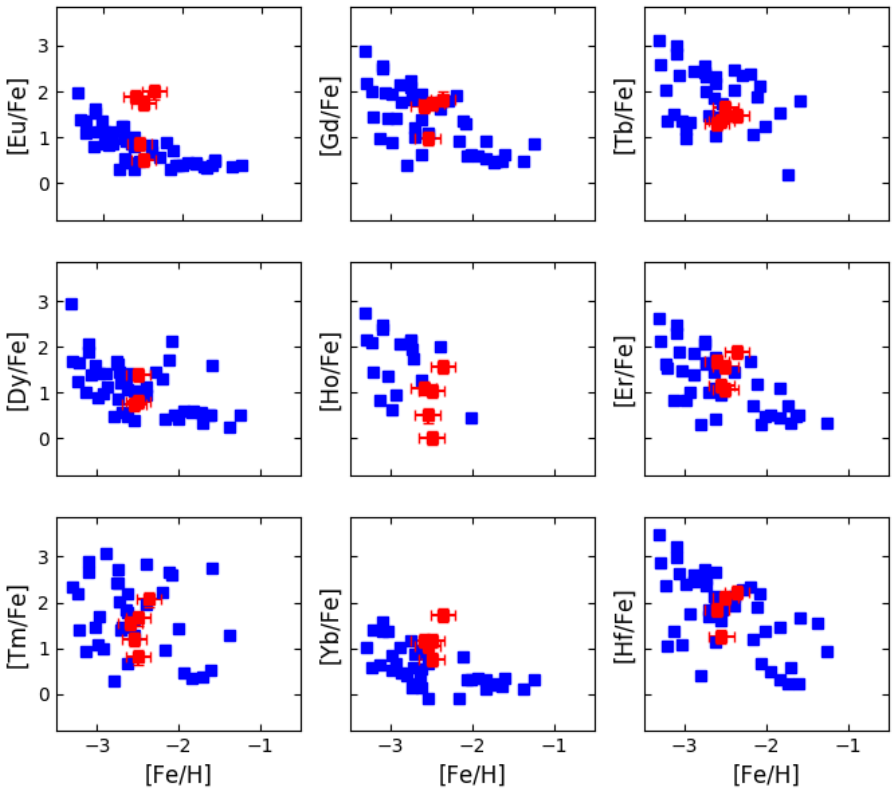

Figure 2: Comparison of the r-process elemental abundance pattern in our five CEMP-rs stars (red squares) with 47 r-process enriched stars from the literature(blue squares).

100 K, 0.5, 0.5 km s^{-2}, and 0.5 dex, respectively, and the corresponding change in abundances are derived. The final uncertainties are then calculated using $\sigma^2_{[\mathrm{X/Fe}]} = \sigma^2_{\mathrm{X}} + \sigma^2_{\mathrm{Fe}}$.

The σ^2_{X} is calculated using the Eq. 2 from Johnson (2002) given by,

$$\sigma^2_{\mathrm{X}} = \sigma^2_{\mathrm{ran}} + \left(\frac{\partial \log \varepsilon}{\partial T}\right)^2 \sigma^2_T + \left(\frac{\partial \log \varepsilon}{\partial \log g}\right)^2 \sigma^2_{\log g} + \left(\frac{\partial \log \varepsilon}{\partial \xi}\right)^2 \sigma^2_\xi.$$

The σ_T, $\sigma_{\log g}$, and σ_ξ are the typical uncertainties on the atmospheric parameters, which are estimated as $\sigma_T = 50$ K, $\sigma_{\log g} = 0.2$ dex, and $\sigma_\xi = 0.05$ km s^{-1}.

3. Discussions and Conclusions

We derived the abundance of Tb, Ho, Tm, and Yb in five CEMP-rs stars. In Fig. 2, the available abundances of r-process elements in our program stars were compared with those in r-process enriched stars which include both rI and rII stars. According to the figure, our program stars exhibit similar abundances for these elements as r-process enriched stars who are similar in metallicity indicating a comparatively higher contribution from i-process sites such as low-mass low-metallicity AGB stars. But the final conclusion should be based on the comparison with model predictions as well as the abundances of these elements in CEMP-s stars.

Acknowledgments

We gratefully acknowledge financial support from the Belgo-Indian Network for Astronomy and astrophysics (BINA), approved by the International Division, Department of Science and Technology (DST, Govt. of India; DST/INT/BELG/P-09/2017) and the Belgian Federal Science Policy Office (BELSPO, Govt. of Belgium; BL/33/IN12). D. K. acknowledges the financial support from the University of Calicut through a seed money grant with file number U.O.No.14449/2022/Admn.

Further Information

Authors' ORCID identifiers

0000-0002-3532-2793 (Drisya KARINKUZHI)
0000-0003-0499-8608 (Sophie VAN ECK)

Author contributions

D. K. and S. V. E. initiated this project. M. R. A. did the analysis. The manuscript was prepared by D. K. and S. V. E.

Conflicts of interest

The authors declare no conflict of interest.

References

Alvarez, R. and Plez, B. (1998) Near-infrared narrow-band photometry of M-giant and Mira stars: models meet observations. A&A, 330, 1109–1119. https://ui.adsabs.harvard.edu/link_gateway/1998A&A...330.1109A/ADS_PDF.

Asplund, M., Grevesse, N., Sauval, A. J. and Scott, P. (2009) The chemical composition of the Sun. ARA&A, 47, 481–522. https://doi.org/10.1146/annurev.astro.46.060407.145222.

Choplin, A., Siess, L. and Goriely, S. (2021) The intermediate neutron capture process. i. development of the *i*-process in low-metallicity low-mass AGB stars. A&A, 648, A119. https://doi.org/10.1051/0004-6361/202040170.

Hampel, M., Karakas, A. I., Stancliffe, R. J., Meyer, B. S. and Lugaro, M. (2019) Learning about the intermediate neutron-capture process from lead abundances. ApJ, 887(1), 11. https://doi.org/10.3847/1538-4357/ab4fe8.

Hampel, M., Stancliffe, R. J., Lugaro, M. and Meyer, B. S. (2016) The intermediate neutron-capture process and carbon-enhanced metal-poor stars. ApJ, 831, 171. https://doi.org/10.3847/0004-637X/831/2/171.

Heiter, U. (2020) Atomic data for stellar spectroscopy. IAUGA, 30, 458–462. https://doi.org/10.1017/S174392131900509X.

Heiter, U., Lind, K., Asplund, M., Barklem, P. S., Bergemann, M., Magrini, L., Masseron, T., Mikolaitis, Š., Pickering, J. C. and Ruffoni, M. P. (2015) Atomic and molecular data for optical stellar spectroscopy. PhyS, 90(5), 054010. https://doi.org/10.1088/0031-8949/90/5/054010.

Johnson, J. A. (2002) Abundances of 30 elements in 23 metal-poor stars. ApJS, 139, 219–247. https://doi.org/10.1086/338117.

Karinkuzhi, D., Van Eck, S., Goriely, S., Siess, L., Jorissen, A., Merle, T., Escorza, A. and Masseron, T. (2021a) Low-mass low-metallicity AGB stars as an efficient *i*-process site explaining CEMP-rs stars. A&A, 645, A61. https://doi.org/10.1051/0004-6361/202038891.

Karinkuzhi, D., Van Eck, S., Jorissen, A., Escorza, A., Shetye, S., Merle, T., Siess, L., Goriely, S. and Van Winckel, H. (2021b) Sr and Ba abundances: Comparing machine-learning with star-by-star analyses. High-resolution re-analysis of suspected LAMOST barium stars. A&A, 654, A140. https://doi.org/10.1051/0004-6361/202141629.

Karinkuzhi, D., Van Eck, S., Jorissen, A., Goriely, S., Siess, L., Merle, T., Escorza, A., Van der Swaelmen, M., Boffin, H. M. J., Masseron, T., Shetye, S. and Plez, B. (2018) When binaries keep track of recent nucleosynthesis. The Zr-Nb pair in extrinsic stars as an s-process diagnostic. A&A, 618, A32. https://doi.org/10.1051/0004-6361/201833084.

Karinkuzhi, D., Van Eck, S., Jorissen, A., Goriely, S., Siess, L., Merle, T. and Masseron, T. (2020) Carbon-enhanced metal-poor stars enriched in s-process and r-process elements. JApA, 41(1), 46. https://doi.org/10.1007/s12036-020-09673-4.